Check for updates

Received: 5 June 2023 | Revised: 15 December 2023 | Accepted: 13 February 2024

DOI: 10.1002/hyp.15112

RESEARCH ARTICLE

WILEY

Exploring landscape and geologic controls on spatial patterning of streambank groundwater discharge in a mixed land use watershed

Kevin E. Jackson[1] | Eric M. Moore[1] | Ashley M. Helton[1,2] | Adam B. Haynes[1] | Janet R. Barclay[3] | Martin A. Briggs[4]

[1]Department of Natural Resources and the Environment, University of Connecticut, Storrs, Connecticut, USA

[2]Center for Environmental Sciences and Engineering, University of Connecticut, Storrs, Connecticut, USA

[3]U.S. Geological Survey, New England Water Science Center, East Hartford, Connecticut, USA

[4]U.S. Geological Survey, Observing Systems Division, Hydrologic Remote Sensing Branch, Storrs, Connecticut, USA

Correspondence
Ashley M. Helton, Department of Natural Resources and the Environment, University of Connecticut, Storrs, CT 06269, USA.
Email: ashley.helton@uconn.edu

Present addresses
Kevin E. Jackson, Appalachian Laboratory, University of Maryland Center for Environmental Science, Frostburg, Maryland, USA; and Adam B. Haynes, Earth and Planetary Sciences Department, University of California Santa Cruz, Santa Cruz, Connecticut, USA.

Funding information
NSF-EAR, Grant/Award Number: 1824820; USDA Hatch project, Grant/Award Number: CONS00938; USGS Toxic Substances Hydrology Program

Abstract

Preferential groundwater discharge features along stream corridors are ecologically important at local and stream network scales, yet we lack quantification of the multi-scale controls on the spatial patterning of groundwater discharge. Here we identify physical attributes that best explain variation in the presence and lateral extent of preferential groundwater discharges along two 5th order streams, the Housatonic and Farmington Rivers, and 32 1st to 4th order reaches across the Farmington River network. We mapped locations of preferential groundwater discharge exposed along streambanks using handheld thermal infrared cameras paired with high-resolution topographic and land use land cover datasets, surficial soil characteristic maps, and depth-to-bedrock geophysical measurements. The unconfined Housatonic River, MA, USA (12 km) had fewer discharge locations and less lateral extent (41 discharge locations with 38 m of active discharge/km of river) compared to the partially confined Farmington River, CT, USA (26 km; 169 discharge locations with 129 m of active discharge/km of river). Using a moving window analysis, we found along both rivers that discharge was more likely to occur where bank slopes were steeper, floodplain extent was narrower, and degree of confinement was higher. Along the Farmington River, groundwater discharge was more likely to occur where saturated hydraulic conductivity was higher and depth-to-bedrock was shallower. Among the 32 stream reaches surveyed (33.2 km of total stream length) within the Farmington River watershed, preferential discharge was observed in all but two stream reaches, varied from 0 to 25% of lateral extent along stream banks (mean = 6%), and was more likely to occur where stream reach slopes were steep, saturated hydraulic conductivity was high, and watershed urbanization was low. Our results show that, though both surface (e.g., topographic, land use land cover) and subsurface (e.g., soil characteristics, bedrock depth) factors control the prevalence of streambank preferential groundwater discharge, the dominant controls vary across valley settings and stream sizes.

This is an open access article under the terms of the Creative Commons Attribution-NonCommercial-NoDerivs License, which permits use and distribution in any medium, provided the original work is properly cited, the use is non-commercial and no modifications or adaptations are made.
© 2024 The Authors. *Hydrological Processes* published by John Wiley & Sons Ltd.

KEYWORDS
groundwater-surface water exchange, remote sensing, river morphology, thermal infrared imagery, water temperature

1 | INTRODUCTION

Groundwater discharge to streams and rivers can define stream temperature and baseflow regimes, create critical wildlife habitat, and supply nutrients or contribute contaminants to surface waters (Brookfield et al., 2021; Hare et al., 2021; Sullivan et al., 2021; Hester & Fox, 2020; Tesoriero et al., 2013; Ebersole et al., 2003). Groundwater discharge varies dramatically in flux rates and spatial extents; for example, preferential groundwater discharge, in contrast to spatially distributed 'diffuse' groundwater gains, can range from discrete discharge points to extensive discharge faces (10s to 100 s of meters) along riverbanks that are exposed at lower flows (Barclay et al., 2022; Briggs, Jackson, et al., 2022; Casas-Mulet et al., 2020; Dugdale et al., 2015). These preferential groundwater discharge features have been recognized for their potential ecological importance at local and network scales (Boulton et al., 2006; Briggs & Hare, 2018; Kurylyk et al., 2014; Sullivan et al., 2021). The occurrence, magnitude, and spatial extent of streambank discharges are typically highly spatially heterogeneous (Dole-Olivier et al., 2019) and are difficult to predict with groundwater modelling (Barclay et al., 2022). Thus, there have been recent efforts to disentangle the multiscale physical controls to allow better prediction of preferential groundwater discharge dynamics (e.g., Casas-Mulet et al., 2020; Dugdale et al., 2015; O'Sullivan et al., 2020).

Surface landforms have long been invoked to conceptually explain spatial patterns of groundwater connectivity to surface waters (Winter et al., 1998). Locally, steep streambanks or streambed slopes can cut across hydraulic gradients and create groundwater discharge across the land surface, while high stream curvature can cause the convergence of groundwater flow paths to streams (Eschbach et al., 2017; Gerlach et al., 2022; Wawrzyniak et al., 2016). At the valley scale, the degree of channel confinement can control the prevalence of groundwater discharge, with partially confined valleys having the highest prevalence of streambank groundwater discharge relative to confined or unconfined settings (Dugdale et al., 2015). Landform-derived metrics, such as topographic wetness (a function of slope and the upstream contributing area; Buttle et al., 2004) and terrain ruggedness (indicative of soil texture properties; Gerlach et al., 2022), have shown promise in identifying features that focus flow toward streams and have become more accurate with the increasing availability of high resolution topographic data.

While surface topography can exert strong controls on the spatial patterning of groundwater discharge, characteristics of underlying soils and bedrock geology are important as well. Gerlach et al. (2022) found that the depths and locations of water bearing geologic formations derived from borehole data predicted the occurrence of groundwater discharges across several salmon bearing streams in Alaska, USA. Gerlach et al. (2022) also found that the occurrence of bedrock outcrops was important in creating hillslope and streambank discharge features. Similarly, O'Sullivan et al. (2020) found that topography better predicted stream temperature when bedrock was homogeneous with high hydraulic conductivity to allow groundwater flow toward streams. Heterogenous bedrock with variable hydraulic conductivity presumably modified topographic controls on the spatial patterning of groundwater discharge, reducing the dominance of land surface controls. Some geologic features may vary somewhat predictably by network position; for example, depth-to-bedrock tends to be shallow across mountain headwaters, where the low permeability bedrock interface serves as a lateral shunt of shallow groundwater to streams, affecting stream temperature variability and maximum temperatures at daily to seasonal timescales (Briggs et al., 2018; Briggs, Goodling, et al., 2022). In valley bottom settings, clay and silt lenses embedded in valley sediments may also drive lateral groundwater flow to rivers (Ó Dochartaigh et al., 2019). However, spatially contiguous geologic data are typically not available to the same extent and resolution as topographic data and subsurface geologic features are generally not predictable at the scale of groundwater flow paths (Barclay et al., 2020). There are numerous publicly available geologic map products, but large-scale, interpolated geologic datasets may not accurately represent the physical controls of groundwater discharge occurrence (Briggs, Jackson, et al., 2022; Dugdale et al., 2015).

Human activities also affect patterns of groundwater connectivity to surface waters. It is well- documented that soil compaction and impervious cover associated with human land development reduce infiltration and recharge to groundwater, potentially lowering water tables and reducing the connectivity between groundwater and surface water (Hardison et al., 2009; Kaushal & Belt, 2012; Ledford et al., 2016; Lerner & Harris, 2009). Groundwater pumping may also directly reduce groundwater connectivity with streams (Barlow & Hess, 1993; de Graaf et al., 2019). Hare et al. (2021) found stream sites that lacked substantial local groundwater influence had higher watershed percent impervious cover and higher values of the Hydrologic Disturbance Index (which accounts for seven human impacts, including water withdrawals, see Falcone et al., 2010). At the same time, there is evidence that urbanization can increase groundwater discharge to surface waters through irrigation, stormwater detention ponds and artificial recharge, and leaking water and sewer lines or storm drain systems (Sharp Jr. et al., 2003). Yet, the majority of studies linking topographic and geologic characteristics with the spatial distribution of groundwater discharge have been conducted along low order streams in predominantly undeveloped watersheds or do not explicitly consider the effects of human activities.

To evaluate how multiscale physical features interact to control the occurrence of groundwater discharge to streams, groundwater discharge features need to be mapped at a resolution and scale to capture local controls across meaningful reach lengths. In this study,

10991085, 2024, 3, Downloaded from https://onlinelibrary.wiley.com/doi/10.1002/hyp.15112, Wiley Online Library on [26/11/2025]. See the Terms and Conditions (https://onlinelibrary.wiley.com/terms-and-conditions) on Wiley Online Library for rules of use; OA articles are governed by the applicable Creative Commons License

we used thermal infrared (TIR) imagery to create high-resolution (1 m) maps of streambank preferential groundwater discharge, building on recently published work from the same Farmington River watershed system (Barclay et al., 2022; Briggs, Jackson, et al., 2022; Haynes et al., 2023; Yearsley et al., 2019). Preferential groundwater discharge is defined by unidirectional groundwater upwelling occurring in discrete patches at a relatively high flux rate such that groundwater temperature signatures are preserved enough to be observed in contrast to water (or streambank) surface temperatures with TIR (Briggs & Hare, 2018). TIR imagery can be used to quickly identify discharge areas across contiguous space in a more complete manner than any other current groundwater/surface water exchange methodology, and therefore has great potential to inform multiscale drivers of the spatial patterns of groundwater discharge (Fullerton et al., 2017; Torgersen et al., 2001).

The goal of this study was to identify physical attributes that best explain the presence and lateral extent of preferential groundwater discharges observed along mainstem rivers and lower order streams. This was accomplished by comprehensively mapping locations of streambank preferential groundwater discharge across stream sizes using handheld TIR surveys (floating and walking) over approximately 70 km of stream length and pairing the resultant discharge maps with high-resolution topographic and satellite-derived land use land cover (LULC) datasets, soil characteristics maps, and depth-to-bedrock measurements. Our specific objectives were to (1) map the spatial distribution of streambank preferential groundwater discharge locations in two mixed land use 5th order river sections that vary in their valley settings (unconfined and partially-confined), (2) quantify the spatial extent of streambank preferential groundwater discharge across headwater and tributary streams draining different dominant land uses, and (3) evaluate topographic, geologic, and LULC controls on the presence and lateral extent of preferential groundwater discharge. Our approach leverages extensive field surveys and publicly available geospatial datasets to quantify inter- and intra-watershed controls on the spatial patterning of preferential groundwater discharge to streams.

2 | MATERIALS AND METHODS

2.1 | Study sites

2.1.1 | Mainstem reaches

We conducted surveys along 5th order (Strahler) mainstem rivers in two adjacent watersheds: a 12 km section of the Housatonic River near Ashley Falls, MA; and a 26 km section of the Farmington River near Tariffville, CT; the latter was included in a recent watershed modelling effort of stream temperature (Yearsley et al., 2019) (Figure 1). Both rivers are underlain by Pleistocene glacial deposits comprised predominantly of till with some reworked alluvium and fine-grained stratified lake sediments (Olcott, 1995; Stone et al., 2005). The rivers are similar in catchment area and accessibility but differ in their valley settings—the Housatonic River is unconfined and the Farmington River is partially confined by bedrock topographic features (Figure 1). The survey length of the reaches varied depending on our ability to access the rivers via canoe.

The study section of the Housatonic River flows north to south with an average annual river flow of 27.1 m^3/sec and a watershed area of 1204 km^2 (U.S. Geological Survey, 2016; USGS gauge 01198125 based on yearly statistics 2008–2019). The Housatonic River valley is underlain by metamorphic Grenville Belt and carbonate Grenville Shelf deposits. The Housatonic River in southwestern Massachusetts experienced glacial diversion near Great Falls resulting in the accumulation of more than 30 m of fine-lake bottom sediment (Patton, 1988), conditions suitable for increased lateral mobility of the Housatonic River. Contemporary LULC along the Housatonic River is predominantly forest with interspersed agricultural land.

The study section of the Farmington River flows south to north with an average annual discharge of 32.3 m^3/sec and a watershed area of 1494 km^2 (U.S. Geological Survey, 2016; USGS gauge 01189995 based on yearly statistics 2008–2019). This section of the Farmington River is partially confined by the Talcott Mountains, a Triassic-Jurassic aged trapp, and underlain by New Haven Arkose sandstone. Unlike the Housatonic River, the mainstem of the Farmington River has more heterogeneous surficial material ranging from fine-grain alluvium to coarse till (Stone et al., 2005). The Farmington mainstem traverses over what was once Lake Farmington, a glacial diversion that resulted in a greater degree of unconsolidated sediment sorting relative to the rest of the watershed. Contemporary LULC along the Farmington River valley is mixed forest, agriculture, and developed (primarily residential).

2.1.2 | Farmington headwaters

To evaluate preferential groundwater discharge variation among different stream sizes, we surveyed 32 headwater and tributary stream reaches (19 1st, 9 2nd, 3 3rd, and 1 4th order streams) throughout the Farmington River watershed (Figure 2). The northwest portion of the watershed is underlain by coarse-grained glacial till and is predominantly forested. The southern portion of the watershed consists of fine-grained glacial till and contains more developed and agricultural land in the suburban area around Hartford, CT. Stream reaches are primarily forested along the stream corridor but were selected to represent a range of developed watershed LULC (0 to 87%). Stream reach survey length varied depending on site accessibility (1038 m mean reach length, range 302–4622 m).

2.2 | Field data collection

2.2.1 | Thermal infrared surveys

We conducted surveys for streambank preferential groundwater discharge using handheld thermal infrared (TIR) cameras (FLIR models e8

10991085, 2024, 3, Downloaded from https://onlinelibrary.wiley.com/doi/10.1002/hyp.15112, Wiley Online Library on [26/11/2025]. See the Terms and Conditions (https://onlinelibrary.wiley.com/terms-and-conditions) on Wiley Online Library for rules of use; OA articles are governed by the applicable Creative Commons License

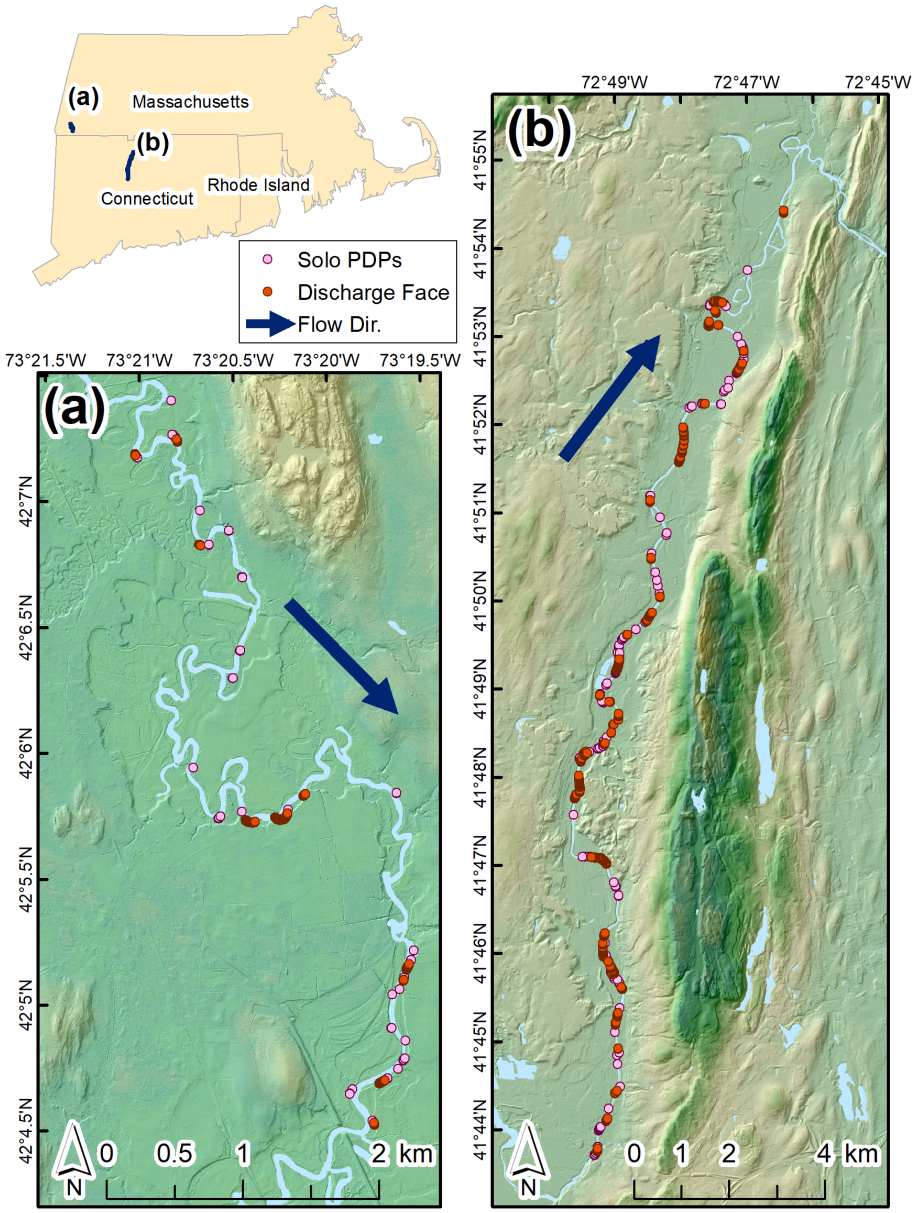

FIGURE 1 The (a) Housatonic River and (b) Farmington River 5th-order study reaches. Preferential groundwater discharges as faces (dark pink, ≥10 m) and as preferential discharge points (PDPs; light pink, <10 m) located with handheld thermal infrared (TIR) cameras. Dark blue arrows indicate flow direction. Inset shows study reach locations. The base maps are hillshades to illustrate the relative confinement of the two river valleys, derived from LiDAR Terrain data from MassGIS (2007) for (a) and from Connecticut Elevation (LiDAR) Data from Connecticut Conditions Online (2016) for (b).

and t540) to identify water line and bank thermal anomalies indicative of discharging groundwater. Early in the study we piloted the use of drone-based TIR imagery to map preferential groundwater discharges and found they were difficult to identify with confidence due to their variable spatial extent and interferences from riparian vegetation cover (Briggs, Jackson, et al., 2022). Therefore, we conducted surveys for bank preferential groundwater discharge in the two 5th order river segments by canoeing within five meters of each bank and in the headwater streams by walking in the center of each stream (1st and 2nd order streams) or by a mix of walking and canoeing (3rd and 4th order streams) and scanning both banks with the TIR cameras (Moore et al., 2023).

Surveys were performed during summer (July–September 2019 and 2020) low flow conditions following Barclay et al., (2022), when surface water temperatures (>15°C) contrast with groundwater temperatures (typically 9–13°C) in New England, USA. We also validated surface and groundwater temperatures directly with digital thermometers (precision 0.1°C) and recorded visible signs of groundwater discharge (e.g., observable flow, presence of upwelling macropores, grain sorting). We recorded groundwater discharge locations using GPS coordinates at the upstream and downstream ends of areas of active groundwater discharge and also measured the longitudinal extent of groundwater discharge along the bank with a measuring tape. We defined preferential groundwater discharge faces to be banks with active groundwater discharge greater than or equal to 10 m in longitudinal extent. Preferential discharge points (PDPs, Briggs, Jackson, et al., 2022) were defined to be less than 10 m in longitudinal extent. We considered groundwater discharges, both PDPs and groundwater discharge faces, to be distinct if separated on both sides (i.e., their upstream and downstream extent) by more than 10 m of inactive streambank. The results of our surveys are 1 m-resolution maps of the presence or absence of preferential groundwater discharge for

10991085, 2024, 3, Downloaded from https://onlinelibrary.wiley.com/doi/10.1002/hyp.15112, Wiley Online Library on [26/11/2025]. See the Terms and Conditions (https://onlinelibrary.wiley.com/terms-and-conditions) on Wiley Online Library for rules of use; OA articles are governed by the applicable Creative Commons License

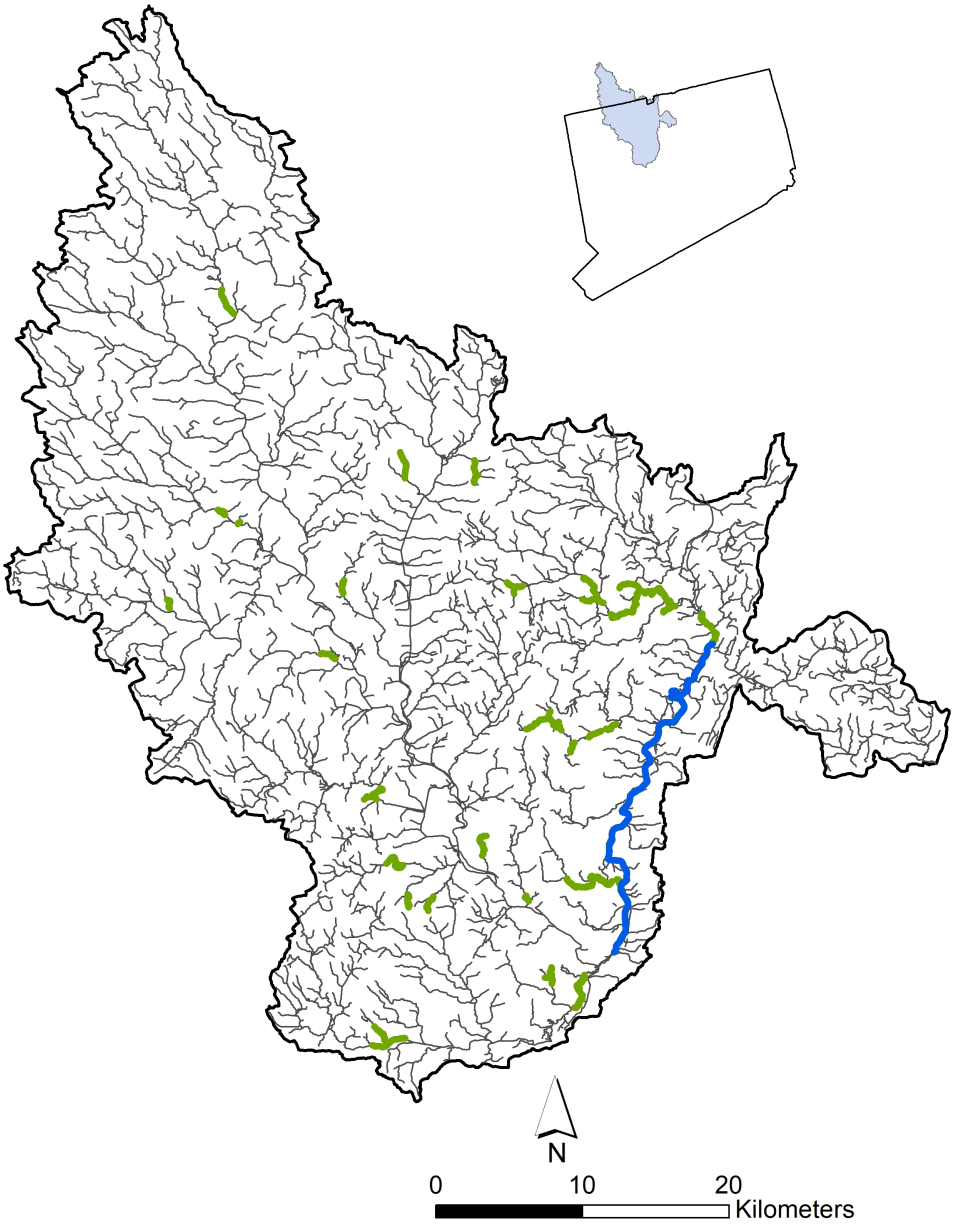

FIGURE 2 1st to 5th order stream reaches surveyed for the presence of preferential groundwater discharge in the Farmington River watershed. 1st to 4th order surveyed stream reaches are highlighted in green. The Farmington River mainstem is highlighted in dark blue (see Figure 1). Red star represents the watershed outlet.

each stream segment surveyed. In total, we surveyed 71 km of stream length for the presence of waterline and streambank groundwater discharge across the Farmington River (26 km) and Housatonic River (12 km) mainstems, and the Farmington River watershed headwaters (33 km across 1st to 4th order streams) (Figures 1 and 2).

2.2.2 | Depth-to-bedrock

To augment existing geologic data along the Farmington River, depth-to-bedrock measurements were collected using passive seismic methods in November 2019 and May 2020 as described in detail by Jackson et al. (2023). Ambient seismic noise data were collected using Model TEP-3C Tromino seismometers. The ratio of horizontal-to-vertical Fourier spectra (HVSR), first proposed by Nakamura (1989), was computed and inverted with shear-wave velocity to estimate the depth-to-bedrock using Grilla software (MOHO, S.R.L.). HVSR is an affordable and effective alternative to active seismic or geotechnical methods that allows researchers to model the depth where lower velocity unconsolidated surface sediment transitions sharply to higher velocity bedrock, particularly in glaciated terrain (Nakamura, 2009). To calculate depth-to-bedrock only two variables are needed (Nakamura, 2019): the averaged shear-wave velocity of the shallow subsurface (typically assumed or measured with active seismic methods) and the resonant frequency determined from HVSR data. Prior research in the Connecticut River Valley provides adequate information regarding subsurface geology to estimate shear wave velocity, as well as some measurements of the parameter (Johnson & Lane, 2016; Stone et al., 2005). The resonant frequency was determined for each location using Grilla software, and bedrock depth

10991085, 2024, 3, Downloaded from https://onlinelibrary.wiley.com/doi/10.1002/hyp.15112, Wiley Online Library on [26/11/2025]. See the Terms and Conditions (https://onlinelibrary.wiley.com/terms-and-conditions) on Wiley Online Library for rules of use; OA articles are governed by the applicable Creative Commons License

measurements were assigned a general reliability rating based on established USGS protocols as described in Jackson et al. (2023).

2.3 | Geospatial datasets and analysis

For the 5th order mainstems, we derived local- and valley-scale topographic variables; subsurface variables (e.g., soil characteristics and depth-to-bedrock); and adjacent LULC from publicly available geospatial datasets based on a variation of a moving window analysis (Hagen-Zanker, 2016). Within ArcMAP (v.10.8.1; ESRI), each mainstem was divided into 50 m increments following the centerline of the river channel. For each 50 m increment as a center point, we specified the window extent (or neighbourhood) for each variable of interest, allowing the windows to overlap, and within which we computed metrics using a variety of vector and raster datasets, as follows:

2.3.1 | Topographic variables

- Mean bankside slope was derived from 1 m-resolution bare-earth digital elevation models (DEMs) based on publicly accessible LiDAR data for both Massachusetts and Connecticut accessed through MassGIS (Bureau of Geographic Information; https://www.mass.gov/orgs/massgis-bureau-of-geographic-information) and Connecticut Environmental Conditions Online (CT ECO; http://www.cteco.uconn.edu/data/lidar/index.htm), respectively. Slope was measured within a 10 m buffer from the streambank for each 50 m stream increment.
- Valley Bottom Extent was calculated as the fraction of valley floor within a 1000 m × 500 m window. We classified a 30 m cell as valley floor if elevations were within 10 m of the minimum 50 m river increment elevation based on a resampled 5 m resolution LiDAR based DEM.
- Floodplain Extent was calculated as the fraction of the floodplain within a 1000 m × 500 m window. We classified a 30 m cell as floodplain if elevations were within 3 m of the minimum 50 m river increment elevation based on a resampled 5 m resolution LiDAR based DEM.
- Confinement was calculated as the fraction streambank length on either bank within a 1000 m × 500 m window that is within 30 m of the floodplain boundary.
- Local curvature was calculated by fitting an arc to cartesian coordinates of the center point of each 50 m river increment and its upstream and downstream neighbouring 50 m increments. Local curvature is the ratio of the distance between (1) the midpoint of the fitted arc and the midpoint of the straight line between center points and (2) the straight-line distance between center points. Higher ratio values correspond to a wider arc.
- Sinuosity was calculated as the ratio between the total stream length within a 1000 m × 500 m window and the shortest Euclidean distance between the furthest upstream and downstream 50 m center points contained within the window.

2.3.2 | Land use/land cover (LULC) variables derived from 30 m resolution National Land Cover Dataset (Dewitz, 2021)

- Percent riparian forest was calculated as the percentage of forested LULC within the intersection of a 50 × 200 m window and a 60 m buffer of the river channel, which meets the minimum area definition posed by the USGS (Johnson & Zelt, 2005).
- Percent riparian developed was calculated as the percent of developed LULC that occurs with the intersection of a 500 × 1000 m window and a 600 m buffer of the river channel. A buffer of 600 m fits within the valley-scale window size and facilitates capture of valley-scale heterogeneity in developed land.

2.3.3 | Subsurface variables

- Soil characteristics were derived from Soil Survey Geographic (SSURGO) database shapefiles (Soil Survey Staff, 2020) joined with tabular data of area- and depth- weighted averages of SSURGO variables using NRCS map unit keys (MUKEY identifications) with a 500 m × 1000 m window extent. We considered soil saturated hydraulic conductivity (KSAT), soil erodibility factor (KFACT), percent soil sand (SAND), and water table depth (WTDEP).
- For the Farmington River mainstem we also evaluated spatial patterns of groundwater discharge relative to depth-to-bedrock measured locally along the river corridor using geophysical methods (see section 2.2.2). We linked 50 m river increments with their nearest neighbouring HVSR field measurement.

For the mainstems, to evaluate spatial patterning of groundwater discharge, we defined three groundwater extent categories using our 50 m increments from the moving window analysis. Each 50 m increment was categorized as (1) having an absence of preferential groundwater discharge if no groundwater discharge was observed, (2) having a limited spatial extent of groundwater discharge if less than 10 m of riverbank had observed groundwater discharge, or (3) having spatially extensive groundwater discharge if 10 m or more of riverbank had observed groundwater discharge. This approach aggregates PDPs and faces into a single dataset. For the 50-meter moving window analysis, we discretized 528 windows (groundwater absent in 346, limited lateral extent in 119, and extensive lateral extent in 63) for the 5th order section of the Farmington. For the Housatonic, we discretized 251 windows (groundwater absent in 216, limited lateral extent in 28, and extensive lateral extent in 7). Figures S1 and S2 show the mapped moving window groundwater extents and all geospatial parameters for the Farmington and Housatonic Rivers, respectively.

For the headwater and tributary streams, instead of the variable window approach, we delineated the watershed upstream of the surveyed reach ending point using the StreamStats tool (U.S. Geological Survey, 2019a). We calculated percent watershed LULC (Dewitz, 2019) for each watershed. Stream reach slope was averaged along each study reach using the National Hydrography Dataset (U.S.

10991085, 2024, 3, Downloaded from https://onlinelibrary.wiley.com/doi/10.1002/hyp.15112, Wiley Online Library on [26/11/2025]. See the Terms and Conditions (https://onlinelibrary.wiley.com/terms-and-conditions) on Wiley Online Library for rules of use; OA articles are governed by the applicable Creative Commons License

Geological Survey, 2019b). This is distinct from streambank slope derived in the mainstem sites and represents the steepness of the channel rather than the streambank. The same SSURGO metrics as the mainstems were derived for the midpoint of each stream reach using MUKEY identifications. We paired these geospatial variables with measured preferential groundwater discharge extent for each reach to evaluate potential physical controls. Because the length of the stream reaches surveyed varied substantially due to variable accessibility, we categorized the reaches based on the proportion of reach length along which we observed groundwater discharge. We categorized each reach as having extensive lateral groundwater discharge (10% or more of surveyed length with visible groundwater seepage, $n = 7$), limited lateral groundwater discharge (between 1% and 10%, $n = 19$), and groundwater discharge absent or <1% ($n = 6$).

2.4 | Statistical analysis

All statistical analyses were performed in R (R Core Team, 2021). For each of the two mainstems, we determined statistically significant differences between groundwater extent categories for geospatial variables (topographic, LULC, and soil characteristics) derived from the moving window analysis and depth-to-bedrock. We used the method of analysis of multiple means described by Herberich et al. (2010), which does not require normality, equal variances, or equal sample sizes. Similarly, for headwaters and tributaries we also followed Herberich et al. (2010) to determine significant differences between groundwater extent categories for geospatial variables derived for the stream reach (slope, soil characteristics) and watershed (LULC).

For the two 5th order rivers with 50 m windows in the extensive groundwater discharge category (i.e., 10 m or greater lateral extent), we also explored the multiscale physical variables described above as drivers of the lateral extent of groundwater discharges. For the unconfined Housatonic River section there were only seven windows with spatially extensive groundwater discharge, so we applied simple linear regression to explore potential physical controls. For the partially confined Farmington River section, there were 62 windows with extensive discharge so we used a multiple linear regression approach to explore potential controls. Multiple linear regression selection was performed with the regsubsets function in the "leaps" package (Lumley, 2020). Regsubsets selects the best candidate model for each possible number of parameters from 2 to 7, including the intercept, with an exhaustive search that includes every combination of parameters at each level. We selected the best fit model as the model with the lowest Akaike's information criterion for small sample sizes (AICc) and considered models within two AICc with model weights greater than 20%. For all parameters, normality was tested with the Shapiro–Wilk Normality Test and natural log transformed as needed to improve normality. We eliminated parameters that were strongly correlated (Pearson's abs(r) >0.60; Figure S3). Our final set of predictor variables was floodplain extent, local curvature (Ln transformed), sinuosity (Ln transformed), bankside slope, forested land cover, developed land cover, KSAT, WTDEP, and depth-to-bedrock.

3 | RESULTS

3.1 | Comparison of mainstem river valleys

For the 5th order mainstems, groundwater discharge was more prevalent along the partially confined Farmington River than the unconfined Housatonic River (Figure 1). Along the Farmington River mainstem we observed 169 unique preferential groundwater discharge features located more than ≥10 m apart along the riverbank. Of the 169 total discharge locations, 104 were classified as PDPs (ranging from 1 to 9 m in extent, median = 1 m) and 65 as discharge faces (ranging from 10 to 238 m in extent, median = 34 m). Along the Housatonic River mainstem we observed 41 distinct groundwater discharge features, of which 31 were classified as PDPs (ranging from 1 to 8 m, median = 1 m) and 10 as discharge faces ranging from 10 to 126 m in length (median = 22 m). Overall, the Farmington River had a greater average density of streambank discharge at 129 m of groundwater discharge features per km of river surveyed compared to the Housatonic River that had 38 m/km.

The Farmington and Housatonic Rivers differed in all analysed geospatial characteristics (Table S1). The Farmington River tended to have steeper and higher banks, narrower valley bottom extent, and more developed LULC than the Housatonic River. The Housatonic River, as is typical of less confined river valleys, had higher convexity (0.112 ± 0.006) and sinuosity (1.89 ± 0.04) than the Farmington River (convexity = 0.029 ± 0.001; sinuosity = 1.18 ± 0.01). The Housatonic River also had more riparian forest cover (69%) and less developed cover (6%) than the Farmington River (61% riparian forest and 32% developed cover). The river valleys also varied by surficial soil characteristics; the Farmington River had higher KSAT, SAND, and WTDEP whereas the Housatonic River had higher KFACT (Table S1).

3.2 | Spatial controls of groundwater discharge along mainstems

Groundwater tended to be present where mean bankside slopes were steeper, floodplain extents were narrower, and confinement was greater for both the Housatonic and Farmington Rivers, regardless of the lateral extent of groundwater discharge (among 50 m moving windows, Table 1 and Figure 3). In the Farmington River, bankside slopes averaged 38.08 (±0.95) where groundwater discharge was present and 29.25 (±0.49) where groundwater discharge was absent. Though slopes were generally lower overall in the Housatonic (Table S1), the pattern was similar. Where groundwater was laterally extensive, slopes were higher (16.72 ± 2.91) than where groundwater was absent (12.93 ± 0.40; Table 1). Both sites showed similar patterns in regard to floodplain extent; laterally extensive groundwater discharge tended to be present when floodplain extent was relatively low (on average 0.46 ± 0.02 and 0.49 ± 0.07 for the Farmington and Housatonic, respectively) and absent when floodplain extent was relatively high (0.58 ± 0.01 and 0.71 ± 0.01). Similarly, groundwater discharge was present when confinement was greater, though confinement was

10991085, 2024, 3, Downloaded from https://onlinelibrary.wiley.com/doi/10.1002/hyp.15112, Wiley Online Library on [26/11/2025]. See the Terms and Conditions (https://onlinelibrary.wiley.com/terms-and-conditions) on Wiley Online Library for rules of use; OA articles are governed by the applicable Creative Commons License

TABLE 1 Mean (std error) of geospatial variables derived for the Farmington and Housatonic Rivers based on the moving window analysis for areas of preferntial groundwater discharge presence and absence.

	Farmington			Housatonic		
		Present			Present	
Variable	Absent	<10 m	≥10 m	Absent	<10 m	≥10 m
Bankside slope (percent rise, unitless)	29.25[a] (0.49)	36.30[b] (0.69)	38.08[b] (0.95)	12.93[a] (0.40)	15.49[b] (1.08)	16.72[ab] (2.91)
Local curvature (ratio)	0.029 (0.002)	0.029 (0.004)	0.025 (0.003)	0.12 (0.007)	0.11 (0.019)	0.12 (0.051)
Valley bottom extent (%)	0.89 (0.01)	0.90 (0.01)	0.86 (0.02)	0.93 (0.01)	0.94 (0.02)	0.98 (0.01)
Floodplain extent (%)	0.58[a] (0.01)	0.51[b] (0.01)	0.46[b] (0.02)	0.71[a] (0.01)	0.59[b] (0.04)	0.49[b] (0.07)
Sinuosity (ratio)	1.19 (0.02)	1.17 (0.05)	1.16 (0.05)	1.93[a] (0.04)	1.65[b] (0.19)	1.55[b] (0.16)
Confinement (%)	0.63[a] (0.02)	0.82[b] (0.02)	0.83[b] (0.03)	0.19[a] (0.01)	0.32[ab] (0.04)	0.36[b] (0.07)
KSAT (μm/s)	58.99[a] (0.72)	62.35[b] (0.99)	63.21[b] (1.62)	31.08 (0.76)	32.69 (2.08)	37.03 (5.70)
KFACT	0.35[a] (0.002)	0.35[a] (0.003)	0.33[b] (0.005)	0.43 (0.004)	0.42 (0.011)	0.41 (0.029)
SAND (%)	65.70[a] (0.28)	67.15[b] (0.40)	68.16[b] (0.53)	48.52 (0.63)	48.27 (1.66)	50.59 (4.38)
WTDEP (cm)	90.91[a] (1.30)	101.40[b] (1.77)	107.59[b] (2.89)	75.35 (1.40)	79.59 (2.38)	76.52 (2.44)
Developed cover (%)	31 (1.1)	33 (2.2)	34 (2.7)	5.9 (0.4)	5.3 (0.9)	2.6 (1.2)
Riparian cover (%)	64[a] (1.4)	56[b] (2.8)	58[ab] (2.8)	70 (1.7)	60 (6.0)	55 (10)
n	346	117	63	214	28	7

Note: Letters indicate significant differences among the groundwater spatial extent categories for each river section at $p < 0.05$. *n* indicates the number of 50 m windows along each river section.
Abbreviations: KFACT, soil erodibility factor; KSAT, saturated hydraulic conductivity; SAND, percent soil sand; WTDEP, water table depth.

lower in the Housatonic than the Farmington; confinement increased from 0.63 ± 0.02 and 0.19 ± 0.01 in the Farmington and Housatonic, respectively, in the absence of groundwater discharge to 0.83 ± 0.03 and 0.36 ± 0.07 where groundwater discharge was laterally extensive. Floodplain extent and confinement were negatively correlated in both the Farmington (Pearson's r = −0.76, Figure S3) and the Housatonic (Pearson's r = − 0.77, Figure S4). In the Farmington River, bankside slope was negatively correlated to both floodplain extent (r = −0.62) and confinement (r = −0.76). In the Housatonic, bankside slope was not correlated with either floodplain extent or confinement, though confinement and floodplain extent were negatively correlated to one another (r = −0.77). Valley bottom extent varied little throughout each mainstem and was not significantly related to the presence of groundwater.

In the unconfined Housatonic, groundwater discharge was present where sinuosity was significantly lower (Table 1; Figure 3). Sinuosity was negatively correlated with confinement (r = −0.70) and positively correlated with floodplain extent (r = 0.62; Figure S4), indicating sinuosity was lower where greater confinement and narrower floodplain extent would be expected to increase the presence of groundwater discharge. Thus, the potential role of sinuosity was difficult to disentangle from other geomorphic controls for the Housatonic. Sinuosity varied less throughout the Farmington and was not related to the presence of groundwater discharge (Figure 3; Table 1). Local curvature was not significantly related to presence of groundwater discharge for either river (Table 1), and neither local curvature nor sinuosity were significantly related to the lateral extent of groundwater discharge faces for the Housatonic (based on simple linear regression models, p > 0.05).

In the Farmington River, the presence of groundwater was significantly related to surficial soil characteristics (Table 1; Figure 4). Both KSAT and SAND were higher where groundwater discharge was present. KSAT and SAND were also strongly correlated (r = 0.95, Figure S3). KFACT was significantly lower where more extensive groundwater faces were present (Table 1); KFACT was also strongly negatively correlated to KSAT (r = −0.71) and SAND (r = −0.84) (Figure S3), which may explain this pattern. Groundwater discharge was also more likely to be present when WTDEP was deep (Table 1). For the Housatonic River, there were no significant relationships between soil characteristics and preferential groundwater discharge (Table 1), even though floodplain extent was correlated with soil characteristics (Figure S4).

In the Farmington River, depth-to-bedrock was also significantly related to the presence of groundwater discharge (Figure 5, Table 1). We estimated depth-to-bedrock for 38 unique locations along the Farmington River (Figure S5). Depths ranged from 18 to 85 m with a median depth of 35.3 m, and distances between analysed river increments and their nearest corresponding HVSR data point ranged from 12 to 1391 m with a median nearest distance of 500 m. When we joined each 50 m river cell with its nearest HVSR measurement, we found that depth-to-bedrock decreased from an average of 46 m in windows without groundwater discharge to 36 m in windows with extensive groundwater discharge, a 10 m difference that exceeds the combined uncertainty of most paired

10991085, 2024, 3, Downloaded from https://onlinelibrary.wiley.com/doi/10.1002/hyp.15112, Wiley Online Library on [26/11/2025]. See the Terms and Conditions (https://onlinelibrary.wiley.com/terms-and-conditions) on Wiley Online Library for rules of use; OA articles are governed by the applicable Creative Commons License

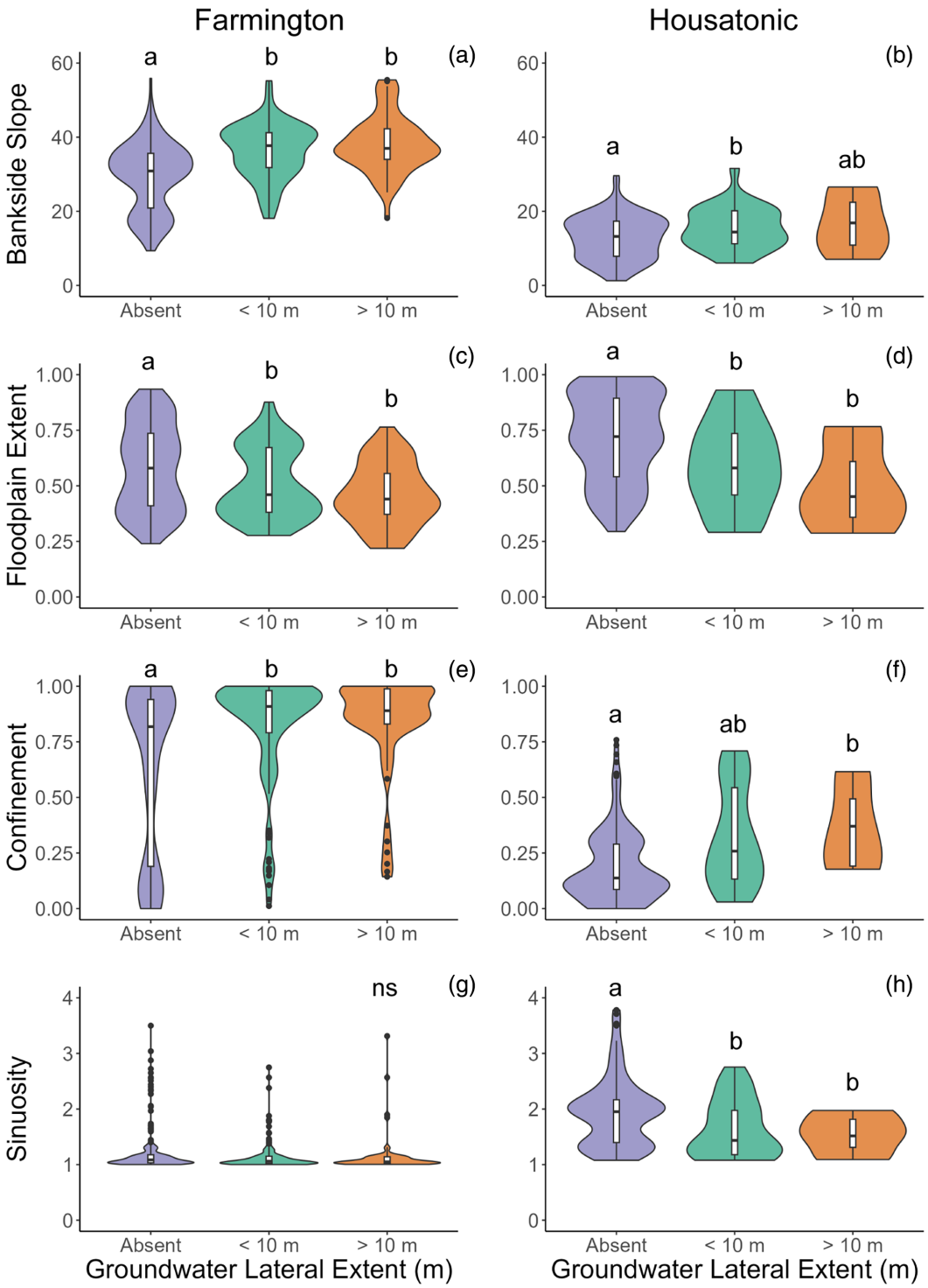

FIGURE 3 Violin plots for bankside slope (percent rise, unitless), floodplain extent (fraction of the floodplain within a 1000 m × 500 m window), confinement (%), and sinuosity (ratio) for the Farmington (a,c,e,g) and Housatonic (b,d,f,h) mainstems for groundwater lateral extent categories (groundwater absent, limited lateral extent <10 m, and extensive lateral extent ≥10 m) based on the 50 m moving window analysis. Lower case letters indicate significant differences among groups as reported in Table 1. ns indicates no significant difference.

measurement comparisons as detailed by Jackson et al. (2023). Depth-to-bedrock was correlated with floodplain extent (Pearson's $r = 0.55$) and confinement ($r = -0.76$) but not with any other geospatial variables.

The best fit models for explaining the percent of the riverbank in the windows with spatially extensive observed groundwater discharge (≥10 m, $n = 63$) in the Farmington included depth- to-bedrock, KSAT, bankside slope, developed cover, and sinuosity (Table 2, Table S3). There were two

10991085, 2024, 3, Downloaded from https://onlinelibrary.wiley.com/doi/10.1002/hyp.15112, Wiley Online Library on [26/11/2025]. See the Terms and Conditions (https://onlinelibrary.wiley.com/terms-and-conditions) on Wiley Online Library for rules of use; OA articles are governed by the applicable Creative Commons License

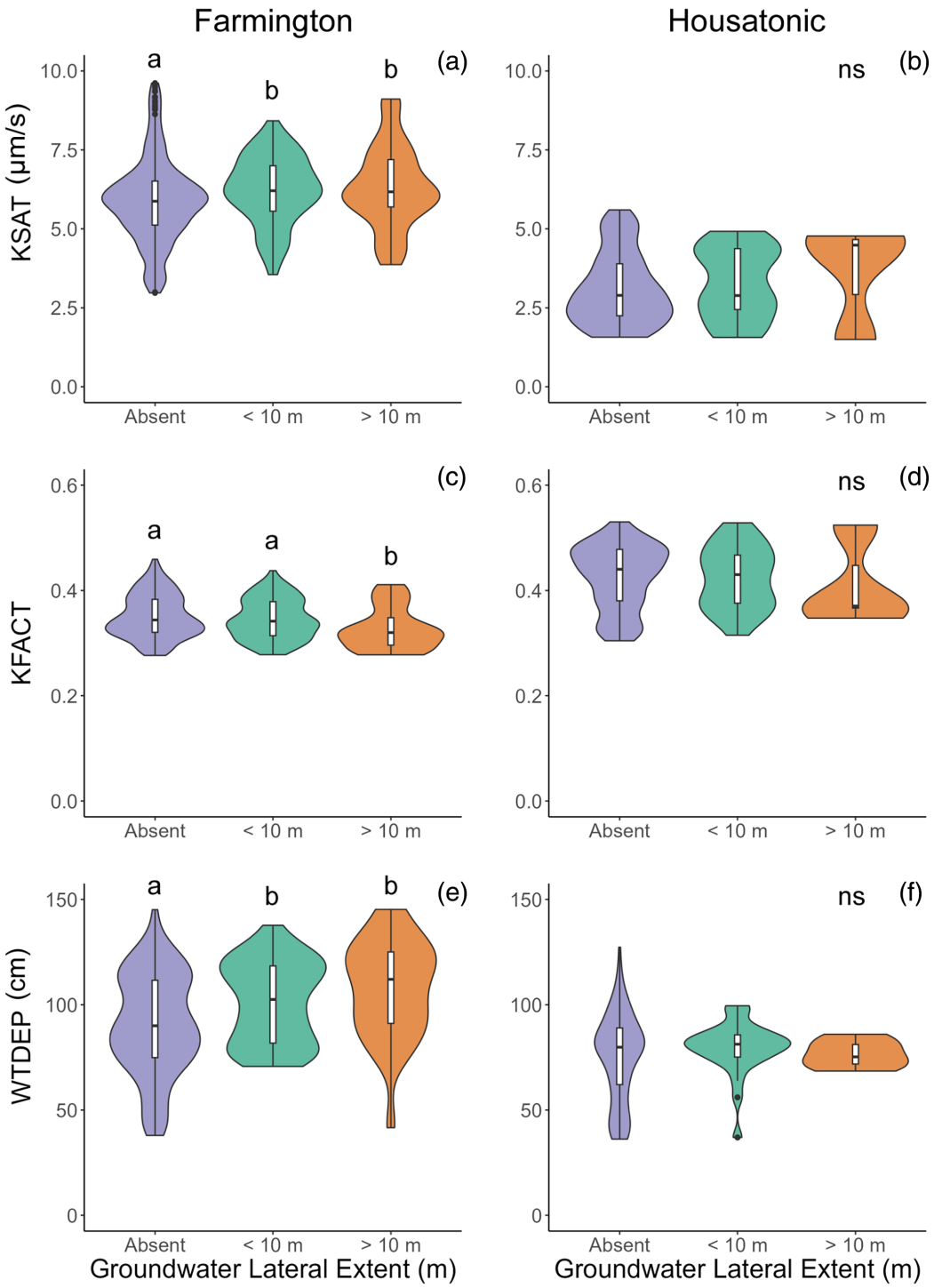

FIGURE 4 Violin plots for Soil Survey Geographic (SSURGO) soil characteristics saturated hydraulic conductivity (KSAT), soil erodibility factor (KFACT), and water table depth (WTDEP) in the Farmington (a,c,e) and Housatonic (b,d,f) mainstems for groundwater lateral extent categories (groundwater absent, limited lateral extent <10 m, and extensive lateral extent ≥10 m) based on the 50 m moving window analysis. Lower case letters represent significant differences among groups as reported in Table 1. ns indicates no significant difference.

models (models 4 and 5 in Table 2) that had model weights greater than 0.20 and similar AICc—the only difference was that the slightly better fitting model included sinuosity, though the model coefficient for sinuosity was not significant (Table S3). The models explained 22 and 24% of the variation in percent groundwater lateral extent within the 50 m windows.

3.3 | Groundwater discharge patterns along headwater and tributary streams

Along headwater and tributary streams to the Farmington River, we found that preferential groundwater discharge was common and

10991085, 2024, 3, Downloaded from https://onlinelibrary.wiley.com/doi/10.1002/hyp.15112, Wiley Online Library on [26/11/2025]. See the Terms and Conditions (https://onlinelibrary.wiley.com/terms-and-conditions) on Wiley Online Library for rules of use; OA articles are governed by the applicable Creative Commons License

observed a wide range of lateral extents of discharging groundwater. Among 1st and 2nd order stream reaches ($n = 28$, 21.6 km surveyed in total) we observed 53 individual groundwater discharge locations, which included 30 PDPs <10 m (2.60 ± 0.46 m) and 23 groundwater seepage faces ranging from 10 to 50 m (23 ± 2.57 m). Only four surveyed 1st and 2nd order stream reaches had no observed streambank groundwater discharge (total surveyed length 1900 m). Two of the four stream reaches without observed groundwater discharge had relatively low KSAT (8.3 and 13.4 μm/s). One of the four was the most urban site (86% of draining watershed was developed land) with relatively low KSAT (24.9 μm/s; Table S2).

Of the four 3rd and 4th order streams surveyed (11.6 km surveyed in total), we observed 142 individual groundwater discharge locations, which included 89 PDPs (3.37 ± 0.30 m) and 53 groundwater discharge faces (27.48 ± 1.81 m). The least extensive groundwater discharge (0.3% of stream length) occurred within the most developed watershed (43% of the watershed is developed land cover) with relatively low KSAT (34 μm/s). Of the other three reaches, the reach with similarly low extent of groundwater discharge (1% of stream length) also had relatively low KSAT (34.5 μm/s) compared to the other two reaches (KSAT = 130 μm/s).

We found that headwater and tributary reaches with more extensive groundwater discharge ($n = 7$) tended to have higher KSAT and SAND (Figure 6, Table 3). KSAT and SAND were strongly correlated with one another ($r = 0.80$; Figure S6). Reaches with higher lateral extent of groundwater discharge also tended to have less development in their watersheds than reaches with limited groundwater discharge extent (Figure 6, Table 3), with groundwater discharge extent ≥10% only observed in watersheds with less than 1.5% developed cover. Streams with limited lateral groundwater discharge ($n = 19$) tended to have higher reach slope and KFACT than streams without groundwater discharge ($n = 6$) or with high groundwater discharge extent.

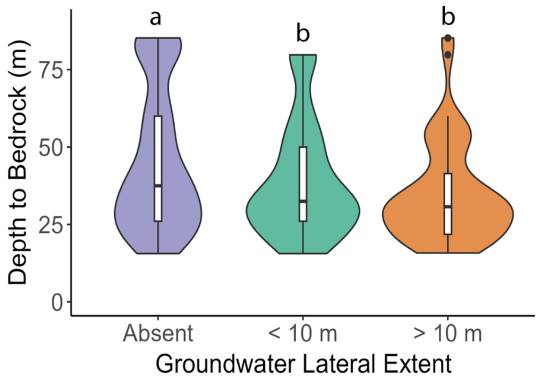

FIGURE 5 Violin plots for depth-to-bedrock for the Farmington River mainstem for groundwater lateral extent categories (groundwater absent, limited lateral extent <10 m, and extensive lateral extent ≥10 m) based on the 50 m moving window analysis. Lower case letters represent significant differences among groups as reported in Table 1.

4 | DISCUSSION

Our results suggest both surface (e.g., topographic, LULC) and subsurface (e.g., soil characteristics, bedrock depth) factors together influence the prevalence of streambank preferential groundwater discharge, but the importance of specific controls varies across valley settings and stream sizes. We found: (1) Topographically, steep local slopes increased the presence of groundwater discharge, with increased groundwater discharge occurring along steeper bank slopes for larger streams and steeper channel slopes for smaller streams. Along larger streams, narrower floodplains and partial confinement also increased the presence of groundwater discharge. (2) Soil characteristics and depth-to-bedrock were related to the presence of groundwater. Particularly, groundwater tended to occur in areas of high saturated hydraulic conductivity and shallow depth-to-bedrock. (3) Smaller streams draining land with higher urbanization had fewer occurrences of preferential groundwater discharge, suggesting features associated with urbanization obscure groundwater discharge or disconnect streams from groundwater. Finally, (4) physical controls strongly correlated to the presence of groundwater discharge were similar regardless of the lateral extent of groundwater discharge along the bank.

TABLE 2 Multiple linear regression model selection for the fraction of lateral groundwater extent in the 50 m windows along the Farmington River mainstem.

Model	K	AIC_c	ΔAIC_c	Wt	R^2_{adj}
1. Depth-to-bedrock	3	23.45	4.85	0.05	0.13
2. Depth-to-bedrock, KSAT	4	25.45	6.85	0.02	0.12
3. Depth-to-bedrock, KSAT, bankside slope	5	21.32	2.71	0.15	0.19
4. Depth-to-bedrock, KSAT, bankside slope, developed cover	6	20.48	1.88	0.22	0.22
5. Depth-to-bedrock, KSAT, bankside slope, developed cover, sinuosity	7	18.61	0.00	0.56	0.24

Note: Models with the lowest Akaike's Information Criterion for small sample sizes (AIC_c) at each parameter level (K) are reported here. We consider best fit models to be those within two AIC_c units from the lowest AIC_c (ΔAIC_c) and model weights (wt) >0.20. We also report the adjusted R^2 (R^2_{adj}) of each model. Coefficients for the best fit models 4 and 5 are reported in Table S3.
Abbreviation: KSAT, saturated hydraulic conductivity.

10991085, 2024, 3, Downloaded from https://onlinelibrary.wiley.com/doi/10.1002/hyp.15112, Wiley Online Library on [26/11/2025]. See the Terms and Conditions (https://onlinelibrary.wiley.com/terms-and-conditions) on Wiley Online Library for rules of use; OA articles are governed by the applicable Creative Commons License

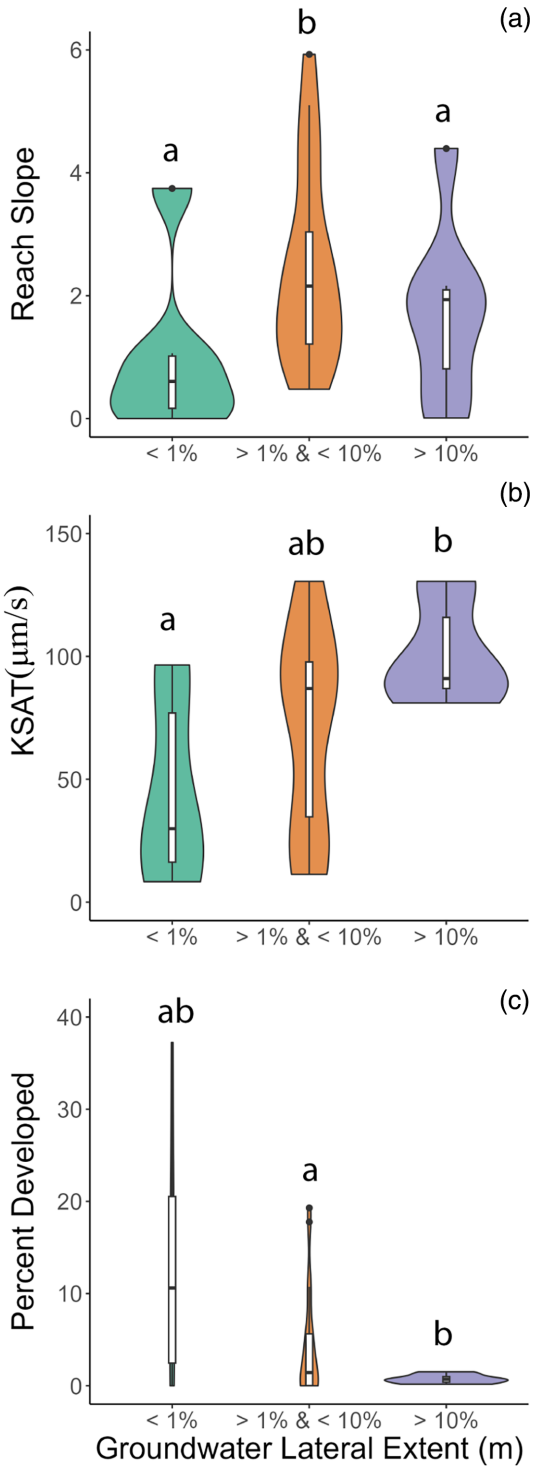

FIGURE 6 Violin plot for channel slope, saturated hydraulic conductivity (KSAT), and watershed percent developed land cover relative to Groundwater Lateral Extent categories for headwater and tributary stream reaches of the Farmington River watershed. Lower case letters represent significant differences among groups as reported in Table 3.

4.1 | Local-to-landscape topographic controls

General differences in the lateral extent of preferential groundwater discharge between the Housatonic and Farmington mainstems confirm well-documented controls of valley setting on the connectivity of ground-and surface-waters. The relatively low topographic and hydraulic gradients of unconfined valleys tend to reduce the likelihood of discharge along exposed stream banksides (Dugdale et al., 2015; O'Brien et al., 2019). Differences in lateral river mobility are apparent between the Housatonic, a river with a wide floodplain and low adjacent topographic gradients, and the Farmington, which is partially confined by the prominent Talcott Mountain bedrock ridge. Even though the overall valley setting varied between the Farmington and Housatonic, the within-river patterns of groundwater discharge were related to variation in valley geomorphology along each mainstem. For both rivers, groundwater discharge along the river was more likely to occur in areas of partial confinement and narrower floodplain extent.

Our findings are consistent with prior research. Winter et al. (1998) conceptually described valleys that are semi-confined or have a moderate entrenchment ratio as having higher densities of groundwater driven cold patches. Dugdale et al. (2015) later confirmed these patterns empirically with large-scale aerial TIR surveys. Here, we build on these previous findings by using high resolution handheld TIR imagery to show how variation in floodplain extent and confinement within individual valleys drive spatial patterns of preferential groundwater discharge. Briggs, Jackson, et al. (2022) found that even low altitude and high spatial resolution mapping with drone TIR tended to miss many riverbank discharges due to riparian tree/root cover (even in winter), so our study design relied on handheld TIR mapping of relatively small features that could be missed by aerial surveys and therefore bias our understanding of dominant physical controls.

Local slope was related to spatial patterning of preferential groundwater discharge across valley settings and stream sizes, though with different context from mainstems to smaller streams. Along the larger streams, incised bank heights generally ranged from a meter or less to approximately 10 meters at cutbanks. In mainstem settings, steeper streambank slopes coincide with locations of preferential groundwater discharge, presumably by directly intersecting the water table where soils are relatively permeable, as described by Winter et al. (1998). However, streambanks were intrinsically less pronounced in the headwaters and along most surveyed tributaries; instead, stream channel slope showed high variability (0.06 to 10%, Table S2). Steeper stream channel slopes coincide with presence of preferential groundwater discharge, likely based on the same saturated zone incision concept driving discharge occurrence along the mainstem banks. Recent analysis of high-resolution stream corridor terrain datasets showed similar findings related to local slope (O'Sullivan et al., 2020), indicating these concepts are robust across scales of inquiry—among rivers, along rivers, and across stream sizes within a network.

For the Farmington River mainstem, the strong association between the presence of groundwater discharge and steep bank slopes may be influenced by the presence of riparian root mass in areas with sharp bank slope breaks, particularly for PDPs (Briggs, Jackson, et al., 2022). Decayed and live roots within riparian areas can create preferential groundwater flow paths (Hester & Fox, 2020). In

10991085, 2024, 3, Downloaded from https://onlinelibrary.wiley.com/doi/10.1002/hyp.15112, Wiley Online Library on [26/11/2025]. See the Terms and Conditions (https://onlinelibrary.wiley.com/terms-and-conditions) on Wiley Online Library for rules of use; OA articles are governed by the applicable Creative Commons License

TABLE 3 Mean (std error) of geospatial variables derived for 1st through 4th order headwater and tributary reaches of the Farmington.

	Lateral groundwater extent		
Variable	**<1%**	**>1% and <10%**	**≥10%**
Stream slope	1.04[a] (0.38)	3.69[b] (0.63)	1.80[a] (0.55)
KSAT (μm/s)	44.8[a] (15.9)	70.9[ab] (9.46)	101.2[b] (7.92)
K Factor	0.50[a] (0.02)	0.37[b] (0.03)	0.38[a] (0.06)
SAND (%)	60[a] (5.5)	70.4[ab] (3.2)	77.4[b] (2.1)
WTDEP (cm)	68 (28)	105 (16)	105 (25)
Percent developed (%)	13.7[ab] (5.87)	4.43[a] (1.38)	0.73[b] (0.19)
n	6	19	7

Note: Letters indicate significant differences among the groundwater spatial extent categories for each river section at $p < 0.05$. *n* indicates the number of surveyed reaches.
Abbreviations: KFACT, soil erodibility factor; KSAT, saturated hydraulic conductivity; SAND, percent soil sand; WTDEP, water table depth.

steep forested hillslopes composed of low permeability glacial tills, common features in the Farmington River watershed, lateral preferential groundwater flow through macropores created by roots, animal burrows, and subsurface erosion is likely. Shallow bedrock fractures can also be a dominant mechanism for groundwater connectivity (Cheng et al., 2017; Sidle et al., 2001), likely influencing discharge patterns in the headwater streams of this study, while large scale permeable bedrock units also contribute to mainstem river spatial patterning when not overlain by thick valley sediments (Haynes et al., 2023).

River curvature is another commonly cited topographic control on groundwater discharge (Larkin & Sharp, 1992; van Balen et al., 2008), with groundwater discharge commonly observed on meanders where bank erosion of sediments cuts into hydraulic head gradients exposing groundwater discharges. Though we qualitatively observed groundwater discharge occurring on the outside of meander bends for both mainstems (Figure 1), sinuosity and local curvature did not seem to be important controlling variables in the overall spatial patterning of groundwater discharge. In the Housatonic, where sinuosity was relatively high, laterally extensive groundwater discharge tended to occur in areas of lower rather than higher sinuosity. Sinuosity was positively correlated with floodplain extent and negatively correlated with confinement (Figure S4), suggesting that even within an unconfined valley, changes in relative confinement along the river valley were important to the occurrence of preferential groundwater discharge.

4.2 | Mapped and measured subsurface controls

We selected the Housatonic and Farmington Rivers because of their different valley settings. Yet, we found that there were also important differences in surficial soil characteristics. Riverbank soils in the Farmington are generally described as 'well' or 'excessively' drained with high sand content, while the Housatonic soils are a mix of 'well', 'moderate', and 'poorly' drained soils (Soil Survey Staff, 2020). Saturated hydraulic conductivity (KSAT), which represents the ability of soil to transport water, was on average two times higher in the Farmington than the Housatonic River valley (Table S1), which could be an additional primary control on the greater presence and lateral extent of preferential groundwater discharge along the Farmington. A similar conclusion was reported by Briggs, Jackson, et al. (2022) for individual PDPs along the same two rivers. Groundwater discharge presence in smaller streams was also linked to soil characteristics, particularly KSAT, which varied widely. KSAT varied across three orders of magnitude—from 8 to 131 um/s—among the headwater and tributary streams and showed a strong positive correlation with reaches where the greatest lateral groundwater extents were observed.

Hydraulic conductivity has long been recognized as a primary driver of groundwater-water exchange dynamics and as an important parameter in predicting groundwater flow from hillslope to regional models (e.g., Brunner et al., 2017; Kalbus et al., 2006) though integrating soil characteristics at spatial scales and resolutions that match those of groundwater discharge measurements has been difficult (e.g., Dugdale et al., 2015; Nauman & Thompson, 2014). Indeed, streambank soil permeability must be high enough to allow preferential discharges that are generally observable via our methods of measuring surface temperature anomalies (groundwater flux rates generally ranging 0.5 to 2 m/d; Haynes et al., 2023). In our prior analysis, we linked only discharge features less than 10 m in lateral extent with the immediately underlying SSURGO features and found that presence of PDPs was not related to local scale soil characteristics (e.g., saturated hydraulic conductivity; Briggs, Jackson, et al., 2022). Here we combined the SSURGO dataset with a coarser resolution (50 m) moving window analysis and our expanded map to include larger discharge faces (≥10 m lateral extent), which better aligned with the resolution of the SSURGO dataset. By better matching our measured and mapped scales, we were able to observe clear relationships between the presence of groundwater discharge and mapped soil characteristics, including KSAT, SAND, and KFACT among river valleys, within the Farmington River valley, and among stream sizes.

Within the Farmington River valley along the mainstem, we found that depth-to-bedrock was shallower where preferential groundwater discharge was present and was the best predictor of the lateral extent of groundwater discharge. Though we were unable to measure depth-

10991085, 2024, 3, Downloaded from https://onlinelibrary.wiley.com/doi/10.1002/hyp.15112, Wiley Online Library on [26/11/2025]. See the Terms and Conditions (https://onlinelibrary.wiley.com/terms-and-conditions) on Wiley Online Library for rules of use; OA articles are governed by the applicable Creative Commons License

to-bedrock using geophysical methods for the Housatonic River, recent interpolated datasets (250 m grid resolution; Hengl et al., 2017) suggest the Housatonic River valley has a mean depth-to-bedrock of 21 m (range 16–31 m) on average 1.5 times deeper than the Farmington River valley (mean 14 m, range 11–18 m). Thus, depth-to-bedrock tended to be shallower where the floodplain was relatively narrow and the valley was more confined both within the Farmington River valley and between the Farmington and Housatonic valley settings, highlighting the potential interactivity in surface and subsurface features in driving the presence of groundwater discharge.

4.3 | Urbanization and preferential groundwater discharge

Urbanization within a watershed fundamentally alters surface and groundwater flowpaths, with changes that have predictable yet variable implications for groundwater surface water connectivity (Sharp Jr. et al., 2003; Walsh et al., 2005). For example, soil compaction and addition of impervious cover can decrease recharge, lowering water tables and disconnecting groundwater from streams. Over-irrigation and leaking water distribution and sewer systems can increase the water table and associated groundwater flow to streams (Han et al., 2017; Hardison et al., 2009; Lerner, 2002; Sharp Jr. et al., 2003; Sytsma et al., 2020). Changes to groundwater-surface water connectivity may vary in magnitude and direction within a watershed or among cities in different climate or geologic settings. Hare et al. (2021) found that streamflow is less likely to show prominent groundwater thermal signatures when draining areas of high impervious cover in an analysis of hundreds of streams across the continental USA. Our results using thermal methods in a New England USA watershed suggest that preferential groundwater discharge is less spatially extensive in streams with >1.5% watershed urban LULC and more likely to be completely absent in streams with >14% urban LULC.

Urban LULC in our watershed was predominantly low and medium intensity development, including houses with septic systems and drinking water wells in exurban suburbs. We found less prevalence of groundwater discharge in the southern portion of the Farmington River watershed along the Pequabuck River near Bristol, CT (surveyed reaches had 43% and 60% watershed developed cover, Table S2). Drinking water within this portion of the watershed is mainly derived from surface water reservoirs rather than from private wells, suggesting that groundwater pumping is not leading to decreasing groundwater discharge. Much of the Pequabuck River watershed consists of altered stream channels (channelization, reinforced banks) that may disconnect groundwater from surface water by altering or obscuring near-stream groundwater flow paths. Seasonal dynamics may also drive observed patterns because urbanization broadly increases the duration and severity of low streamflow events across the USA; late summer droughts may lower the water table more in urban than in forested watersheds (Dudley et al., 2020).

4.4 | Lateral extent of groundwater discharge

Though the lateral extent of groundwater discharges along stream banks varied from <1 m to 238 m, we found that variation in lateral extent did not appear to correlate significantly with groundwater discharge presence. This may be because both our moving window analysis for the mainstems and reach-scale analysis for smaller streams effectively lumped groundwater expressions of varying lateral extent together, masking some of the differences in drivers of individual groundwater discharge points versus more laterally extensive groundwater faces. It may also be because PDPs could be indicative of more expansive groundwater discharge features, even if those features were not visible using our TIR approach, either because of mixing with surface water or discharge below the waterline. Two notable differences were the relationships between lateral extent and surrounding urban LULC and KSAT for headwaters and tributaries (Figure 6). In other words, stream reaches with >10% of their streambanks actively discharging preferential groundwater consistently had both high KSAT and low watershed development.

4.5 | Mapping groundwater discharge in diverse environments

The handheld TIR survey approach used here enables high resolution, efficient identification of bankside preferential groundwater discharge. There are important considerations and limitations of this approach for use across diverse settings to map groundwater discharge. First, handheld TIR surveys (much like airborne surveys, e.g., Harvey et al., 2019; Dugdale et al., 2015) measure surface temperatures, potentially missing discharge below the waterline, particularly during warm summer months when cooler, denser groundwater sinks or during higher flows when thermal signals are quickly mixed. Thus, these methods tend to best capture areas of relatively high (preferential) groundwater discharge at or above the water line. Efforts to conduct surveys during baseflow conditions minimize this limitation; however, our field observations of upwelling macropores along the riverbed, particularly along the Housatonic River, suggest that careful consideration of pairing handheld surveys with towed channel electrical conductivity and geophysical mapping (Gibson et al., 2013) or submersible temperature sensitive fibre optic cables (Hare et al., 2015) should be considered when significant streambed preferential groundwater discharge is expected. Second, the TIR survey method only captures preferential groundwater discharge signals that are thermally distinct from the bankside and interacting surface water; it does not necessarily capture shallow groundwater flow that may have temperatures more similar to air temperature or low flux discharges more susceptible to atmospheric warming and cooling and rapid mixing with surface water. While cold groundwater is of principal concern for systems impacted by warming waters (Nijssen et al., 2001), considering the overall impact of groundwater discharge, including its effect on chemical water quality, requires including

10991085, 2024, 3, Downloaded from https://onlinelibrary.wiley.com/doi/10.1002/hyp.15112, Wiley Online Library on [26/11/2025]. See the Terms and Conditions (https://onlinelibrary.wiley.com/terms-and-conditions) on Wiley Online Library for rules of use; OA articles are governed by the applicable Creative Commons License

evaluation of groundwater discharge with temperatures nearer to that of its interacting surface water. As such, future efforts focused on the spatial patterning of these warmer preferential groundwater discharges could help clarify the overall effects of groundwater discharge.

5 | CONCLUSIONS

Here we show that controls of the spatial patterning of groundwater presence are driven by multiscale factors that include topographic, geologic, and land use land cover variables across stream sizes in a mixed land use watershed and in two contrasting river valleys (partially confined, high hydraulic conductivity versus relatively unconfined, lower hydraulic conductivity). Across stream sizes, presence of preferential groundwater discharge was observed in all stream reaches, except highly urban or low hydraulic conductivity settings where groundwater discharge had minimal lateral extent or was absent. Predicting patterns of groundwater discharge has been an elusive target for the research community; this work sheds critical light on the key drivers of discharge across scales and stream sizes and can inform future predictive modelling in less-sampled space, particularly as new high resolution remote sensing, LiDAR, and geologic datasets are quickly becoming publicly available.

ACKNOWLEDGEMENTS

This work was supported by NSF-EAR award #1824820 to AMH and MAB, USDA Hatch project CONS00938 to AMH, and the USGS Toxic Substances Hydrology Program for MAB and ABH. We thank Fiona Liu, Huayile Zhang, Kenneth Bell, Jason Klimek, and Mark Harvey for their assistance in the field. Any use of trade, firm, or product names is for descriptive purposes only and does not imply endoresement by the U.S. Government.

DATA AVAILABILITY STATEMENT

All data used in this manuscript are publicly available. Data collected as part of the manuscript include depth-to-bedrock (10.5066/P9FTZ0DK) and preferential groundwater discharge locations (10.5066/P915E8JY). The code and file structure used to replicate the moving window analysis are available through Dryad (10.5061/dryad.xsj3tx9mn).

ORCID

Ashley M. Helton https://orcid.org/0000-0001-6928-2104
Martin A. Briggs https://orcid.org/0000-0003-3206-4132

REFERENCES

Barclay, J. R., Briggs, M. A., Moore, E. M., Starn, J. J., Hanson, A. E. H., & Helton, A. M. (2022). Where groundwater seeps: Evaluating modeled groundwater discharge patterns with thermal infrared surveys at the river-network scale. *Advances in Water Resources*, *160*, 104108. https://doi.org/10.1016/j.advwatres.2021.104108

Barclay, J. R., Starn, J. J., Briggs, M. A., & Helton, A. M. (2020). Improved prediction of management-relevant groundwater discharge characteristics throughout river networks. *Water Resources Research*, *56*, e2020WR028027. https://doi.org/10.1029/2020WR028027

Barlow, P. M., & Hess, K. M. (1993). Simulated hydrologic responses of the Quashnet River stream-aquifer system to proposed ground-water withdrawals, Cape Cod, Massachusetts. *US Department of the Interior, US Geological Survey*, *93*(4064). https://doi.org/10.3133/wri934064

Boulton, A. J., Hancock, P. J., Boulton, A. J., & Hancock, P. J. (2006). Rivers as groundwater-dependent ecosystems: A review of degrees of dependency, riverine processes and management implications. *Australian Journal of Botany*, *54*, 133–144. https://doi.org/10.1071/BT05074

Briggs, M. A., Goodling, P., Johnson, Z. C., Rogers, K. M., Hitt, N. P., Fair, J. B., & Snyder, C. D. (2022). Bedrock depth influences spatial patterns of summer baseflow, temperature and flow disconnection for mountainous headwater streams. *Hydrology and Earth System Sciences*, *26*, 3989–4011. https://doi.org/10.5194/hess-26-3989-2022

Briggs, M. A., & Hare, D. K. (2018). Explicit consideration of preferential groundwater discharges as surface water ecosystem control points. *Hydrological Processes*, *32*, 2435–2440. https://doi.org/10.1002/hyp.13178

Briggs, M. A., Jackson, K. E., Liu, F., Moore, E. M., Bisson, A., & Helton, A. M. (2022). Exploring local riverbank sediment controls on the occurrence of preferential groundwater discharge points. *Water*, *14*, 11. https://doi.org/10.3390/w14010011

Briggs, M. A., Lane, J. W., Snyder, C. D., White, E. A., Johnson, Z. C., Nelms, D. L., & Hitt, N. P. (2018). Shallow bedrock limits groundwater seepage-based headwater climate refugia. *Limnologica, Special Issue on Aquatic Interfaces and Linkages: An Emerging Topic of Interdisciplinary Research*, *68*, 142–156. https://doi.org/10.1016/j.limno.2017.02.005

Brookfield, A. E., Hansen, A. T., Sullivan, P. L., Czuba, J. A., Kirk, M. F., Li, L., Newcomer, M. E., & Wilkinson, G. (2021). Predicting algal blooms: Are we overlooking groundwater? *Science of the Total Environment*, *769*, 144442. https://doi.org/10.1016/j.scitotenv.2020.144442

Brunner, P., Therrien, R., Renard, P., Simmons, C. T., & Franssen, H.-J. H. (2017). Advances in understanding river-groundwater interactions. *Reviews of Geophysics*, *55*, 818–854. https://doi.org/10.1002/2017RG000556

Buttle, J. M., Dillon, P. J., & Eerkes, G. R. (2004). Hydrologic coupling of slopes, riparian zones and streams: An example from the Canadian shield. *Journal of Hydrology*, *287*, 161–177. https://doi.org/10.1016/j.jhydrol.2003.09.022

Casas-Mulet, R., Pander, J., Ryu, D., Stewardson, M., & Geist, J. (2020). Unmanned aerial vehicle (UAV)-based thermal infra-red (TIR) and optical imagery reveals multi-spatial scale controls of cold-water areas over a groundwater-dominated riverscape. *Front. Environmental Sciences*, *8*(64). https://doi.org/10.3389/fenvs.2020.00064

Cheng, Y., Ogden, F. L., & Zhu, J. (2017). Earthworms and tree roots: A model study of the effect of preferential flow paths on runoff generation and groundwater recharge in steep, saprolitic, tropical lowland catchments. *Water Resources Research*, *53*, 5400–5419. https://doi.org/10.1002/2016WR020258

Connecticut Environmental Conditions Online. (2016). 2016 Aerial imagery. Retrieved from http://cteco.uconn.edu/data/flight2016/index.htm

de Graaf, I. E. M., Gleeson, T., van Beek (Rens), L. P. H., Sutanudjaja, E. H., & Bierkens, M. F. P. (2019). Environmental flow limits to global groundwater pumping. *Nature*, *574*, 90–94. https://doi.org/10.1038/s41586-019-1594-4

Dewitz, J. (2019). National Land Cover Database (NLCD) 2016 Products [Data set]. U.S. Geological Survey. https://doi.org/10.5066/P9KZCM54

Dewitz, J. (2021). National Land Cover Database (NLCD) 2019 Products [Data set]. U.S. Geological Survey. https://doi.org/10.5066/P9KZCM54

Dole-Olivier, M.-J., Wawzyniak, V., des Châtelliers, M. C., & Marmonier, P. (2019). Do thermal infrared (TIR) remote sensing and direct hyporheic measurements (DHM) similarly detect river-groundwater exchanges? Study along a 40 km-section of the Ain River (France). *Science of the Total Environment*, *646*, 1097–1110. https://doi.org/10.1016/j.scitotenv.2018.07.294

10991085, 2024, 3, Downloaded from https://onlinelibrary.wiley.com/doi/10.1002/hyp.15112, Wiley Online Library on [26/11/2025]. See the Terms and Conditions (https://onlinelibrary.wiley.com/terms-and-conditions) on Wiley Online Library for rules of use; OA articles are governed by the applicable Creative Commons License

Dudley, R. W., Hirsch, R. M., Archfield, S. A., Blum, A. G., & Renard, B. (2020). Low streamflow trends at human-impacted and reference basins in the United States. *Journal of Hydrology*, *580*, 124254. https://doi.org/10.1016/j.jhydrol.2019.124254

Dugdale, S. J., Bergeron, N. E., & St-Hilaire, A. (2015). Spatial distribution of thermal refuges analysed in relation to riverscape hydromorphology using airborne thermal infrared imagery. *Remote Sensing of Environment*, *160*, 43–55. https://doi.org/10.1016/j.rse.2014.12.021

Ebersole, J. L., Liss, W. J., & Frissell, C. A. (2003). Cold water patches in warm streams: Physicochemical characteristics and the influence of SHADING1. *JAWRA Journal of the American Water Resources Association*, *39*(2), 355–368. https://doi.org/10.1111/J.1752-1688.2003.TB04390.X

Eschbach, D., Piasny, G., Schmitt, L., Pfister, L., Grussenmeyer, P., Koehl, M., Skupinski, G., & Serradj, A. (2017). Thermal-infrared remote sensing of surface water–groundwater exchanges in a restored anastomosing channel (upper Rhine River, France). *Hydrological Processes*, *31*, 1113–1124. https://doi.org/10.1002/hyp.11100

Falcone, J. A., Carlisle, D. M., & Weber, L. C. (2010). Quantifying human disturbance in watersheds: Variable selection and performance of a GIS-based disturbance index for predicting the biological condition of perennial streams. *Ecological Indicators*, *10*, 264–273.

Fullerton, A. H., Torgersen, C. E., Lawler, J. J., Steel, E. A., Ebersole, J. L., & Lee, S. Y. (2017). Longitudinal thermal heterogeneity in rivers and refugia for coldwater species: Effects of scale and climate change. *Aquatic Sciences*, *80*, 3–15. https://doi.org/10.1007/s00027-017-0557-9

Gerlach, M. E., Rains, K. C., Guerrón-Orejuela, E. J., Kleindl, W. J., Downs, J., Landry, S. M., & Rains, M. C. (2022). Using remote sensing and machine learning to locate groundwater discharge to Salmon-bearing streams. *Remote Sensing*, *14*, 63. https://doi.org/10.3390/rs14010063

Gibson, J. J., Fennell, J., Birks, S. J., Yi, Y., Moncur, M. C., Hansen, B., & Jasechko, S. (2013). Evidence of discharging saline formation water to the Athabasca River in the oil sands mining region, northern Alberta. *Canadian Journal of Earth Sciences*, *50*, 1244–1257.

Hagen-Zanker, A. (2016). A computational framework for generalized moving windows and its application to landscape pattern analysis. *International Journal of Applied Earth Observation and Geoinformation*, *44*, 205–216. https://doi.org/10.1016/j.jag.2015.09.010

Han, D., Currell, M. J., Cao, G., & Hall, B. (2017). Alterations to groundwater recharge due to anthropogenic landscape change. *Journal of Hydrology*, *554*, 545–557. https://doi.org/10.1016/j.jhydrol.2017.09.018

Hardison, E. C., O'Driscoll, M. A., DeLoatch, J. P., Howard, R. J., & Brinson, M. M. (2009). Urban land use, channel incision, and water table decline along coastal plain streams, north Carolina1. *JAWRA Journal of the American Water Resources Association*, *45*, 1032–1046. https://doi.org/10.1111/j.1752-1688.2009.00345.x

Hare, D. K., Briggs, M. A., Rosenberry, D. O., Boutt, D. F., & Lane, J. W. (2015). A comparison of thermal infrared to fiber-optic distributed temperature sensing for evaluation of groundwater discharge to surface water. *Journal of Hydrology*, *530*, 153–166. https://doi.org/10.1016/j.jhydrol.2015.09.059

Hare, D. K., Helton, A. M., Johnson, Z. C., Lane, J. W., & Briggs, M. A. (2021). Continental-scale analysis of shallow and deep groundwater contributions to streams. *Nature Communications*, *12*, 1450. https://doi.org/10.1038/s41467-021-21651-0

Harvey, M. C., Hare, D. K., Hackman, A., Davenport, G., Haynes, A. B., Helton, A., Lane, J. W., & Briggs, M. A. (2019). Evaluation of stream and wetland restoration using UAS-based thermal infrared mapping. *Water*, *11*, 1568. https://doi.org/10.3390/w11081568

Haynes, A. B., Briggs, M. A., Moore, E., Rey, D. M., Jackson, K., & Helton, A. M. (2023). *Riverbank vertical temperature profiler data and calculated groundwater discharge flux estimates from the Farmington River corridor*. US Geological Survey data release. https://doi.org/10.5066/P9B3CYWW

Hengl, T., Mendes de Jesus, J., Heuvelink, G. B. M., Ruiperez Gonzalez, M., Kilibarda, M., Blagotić, A., Shangguan, W., Wright, M. N., Geng, X., Bauer-Marschallinger, B., Guevara, M. A., Vargas, R., MacMillan, R. A., Batjes, N. H., Leenaars, J. G. B., Ribeiro, E., Wheeler, I., Mantel, S., & Kempen, B. (2017). SoilGrids250m: Global gridded soil information based on machine learning. *PLoS One*, *12*(2), e0169748. https://doi.org/10.1371/journal.pone.0169748

Herberich, E., Sikorski, J., & Hothorn, T. (2010). A robust procedure for comparing multiple means under heteroscedasticity in unbalanced designs. *PLoS One*, *5*, e9788. https://doi.org/10.1371/journal.pone.0009788

Hester, E. T., & Fox, G. A. (2020). Preferential flow in riparian groundwater: Gateways for watershed solute transport and implications for water quality management. *Water Resources Research*, *56*, e2020WR028186. https://doi.org/10.1029/2020WR028186

Jackson, K. E., Haynes, A. B., & Briggs, M. A. (2023). *Passive seismic depth to bedrock data collected along streams of the Farmington River watershed*. U.S. Geological Survey data release. https://doi.org/10.5066/P9FTZ0DK

Johnson, C., & Lane, J. (2016). Statistical comparison of methods for estimating sediment thickness from horizontal-to-vertical spectral ratio (hvsr) seismic methods: An example from Tylerville. In *Symposium on the application of geophysics to engineering and environmental problems 2016, symposium on the application of geophysics to engineering and environmental problems proceedings. Society of Exploration Geophysicists and Environment and engineering geophysical society* (pp. 317–323). Environmental & Engineering Geophysical Society. https://doi.org/10.4133/SAGEEP.29-057

Johnson, M. R., & Zelt, R. B. (2005). Protocols for mapping and characterizing land use/land cover in riparian zones. USGS Open File Report 2005-1302. https://pubs.usgs.gov/of/2005/1302/

Kalbus, E., Reinstorf, F., & Schirmer, M. (2006). Measuring methods for groundwater – surface water interactions: A review. *Hydrology and Earth System Sciences*, *10*, 873–887. https://doi.org/10.5194/hess-10-873-2006

Kaushal, S. S., & Belt, K. T. (2012). The urban watershed continuum: Evolving spatial and temporal dimensions. *Urban Ecosystem*, *15*, 409–435. https://doi.org/10.1007/s11252-012-0226-7

Kurylyk, B. L., MacQuarrie, K. T. B., Linnansaari, T., Cunjak, R. A., & Curry, R. A. (2014). Preserving, augmenting, and creating cold-water thermal refugia in rivers: Concepts derived from research on the Miramichi River, New Brunswick (Canada). https://doi.org/10.1002/eco.1566

Larkin, R. G., & Sharp, J. M. (1992). On the relationship between river-basin geomorphology, aquifer hydraulics, and ground-water flow direction in alluvial aquifers. *GSA Bulletin*, *104*, 1608–1620. https://doi.org/10.1130/0016-7606(1992)104<1608:OTRBRB>2.3.CO;2

Ledford, S. H., Lautz, L. K., & Stella, J. C. (2016). Hydrogeologic processes impacting storage, fate, and transport of chloride from road salt in urban riparian aquifers. *Environmental Science & Technology*, *50*, 4979–4988. https://doi.org/10.1021/acs.est.6b00402

Lerner, D. N. (2002). Identifying and quantifying urban recharge: A review. *Hydrogeology Journal*, *10*(1), 143–152. https://doi.org/10.1007/s10040-001-0177-1

Lerner, D. N., & Harris, B. (2009). The relationship between land use and groundwater resources and quality. *Land Use Policy*, *Land Use Futures*, *26*, S265–S273. https://doi.org/10.1016/j.landusepol.2009.09.005

Lumley, T. based on Fortran code by Miller, A. (2020). Leaps: Regression Subset Selection. R package version 3.1. https://CRAN.R-project.org/package=leaps

MassGIS. (2007). MassGIS Data: New England Boundaries. Available at: https://www.mass.gov/info-details/massgis-data-new-england-boundaries#attributes

Moore, E. M., Jackson, K. E., Haynes, A. B., Harvey, M., Helton, A. M., & Briggs, M. A. (2023). Thermal infrared images of groundwater

10991085, 2024, 3, Downloaded from https://onlinelibrary.wiley.com/doi/10.1002/hyp.15112, Wiley Online Library on [26/11/2025]. See the Terms and Conditions (https://onlinelibrary.wiley.com/terms-and-conditions) on Wiley Online Library for rules of use; OA articles are governed by the applicable Creative Commons License

discharge zones in the Farmington and Housatonic River watersheds (Connecticut and Massachusetts, 2019) (ver. 3.0, January 2023): U.S. Geological Survey Data Release. https://doi.org/10.5066/P915E8JY

Nakamura, Y. (1989). A method for dynamic characteristics estimation of subsurface using microtremor on the ground surface. *Quarterly Report of Railway Technical Research Institute*, *30*, 25–33.

Nakamura, Y. (2009). Basic structure of QTS (HVSR) and examples of applications. In M. Mucciarelli, M. Herak, & J. Cassidy (Eds.), *Increasing seismic safety by combining engineering technologies and seismological data, NATO science for peace and security series C: Environmental security* (pp. 33–51). Springer Netherlands. https://doi.org/10.1007/978-1-4020-9196-4_4

Nakamura, Y. (2019). What is the Nakamura method? *Seismological Research Letters*, *90*, 1437–1443. https://doi.org/10.1785/0220180376

Nauman, T. W., & Thompson, J. A. (2014). Semi-automated disaggregation of conventional soil maps using knowledge driven data mining and classification trees. *Geoderma*, *213*, 385–399. https://doi.org/10.1016/j.geoderma.2013.08.024

Ó Dochartaigh, B. É., Archer, N. A. L., Peskett, L., MacDonald, A. M., Black, A. R., Auton, C. A., Merritt, J. E., Gooddy, D. C., & Bonell, M. (2019). Geological structure as a control on floodplain groundwater dynamics. *Hydrogeology Journal*, *27*, 703–716. https://doi.org/10.1007/s10040-018-1885-0

O'Brien, G. R., Wheaton, J. M., Fryirs, K., Macfarlane, W. W., Brierley, G., Whitehead, K., Gilbert, J., & Volk, C. (2019). Mapping valley bottom confinement at the network scale. *Earth Surface Processes and Landforms*, *44*, 1828–1845. https://doi.org/10.1002/esp.4615

Olcott, P. (1995). HA 730-M ground water atlas of the United States.

O'Sullivan, A. M., Devito, K. J., Ogilvie, J., Linnansaari, T., Pronk, T., Allard, S., & Curry, R. A. (2020). Effects of topographic resolution and geologic setting on spatial Statistical River temperature models. *Water Resources Research*, *56*, e2020WR028122. https://doi.org/10.1029/2020WR028122

Patton, P. C. (1988). Geomorphic response of streams to floods in the glaciated terrain of southern New England. In V. R. Baker, R. C. Kochel, & P. C. Patton (Eds.), *Flood geomorphology* (pp. 261–277). Wiley.

R Core Team. (2021). R: A language and environment for statistical computing. R Foundation for Statistical Computing, Vienna, Austria. https://www.R-project.org/

Sharp, J. M., Jr., Krothe, J. N., Mather, J. D., Gracia-Fresca, B., & Stewart, C. A. (2003). Effects of urbanization on groundwater systems. In *Earth science in the City: A reader* (pp. 257–278). American Geophysical Union (AGU). https://doi.org/10.1029/SP056p0257

Sidle, R. C., Noguchi, S., Tsuboyama, Y., & Laursen, K. (2001). A conceptual model of preferential flow systems in forested hillslopes: Evidence of self-organization. *Hydrological Processes*, *15*, 1675–1692. https://doi.org/10.1002/hyp.233

Soil Survey Staff. (2020). Natural Resources Conservation Service, United States Department of AgricultureWeb Soil Survey. Available online at https://websoilsurvey.nrcs.usda.gov/. Accessed (October 4, 2021)

Stone, J. R., Schafer, J. P., London, E. H., DiGiacomo-Cohen, M. L., Lewis, R. S., & Thompson, W. B. (2005). *Quaternary geologic map of Connecticut and long island sound basin* (p. 2784). U.S. Geological Survey. Scientific Investigations Map. https://doi.org/10.3133/sim2784

Sullivan, C. J., Vokoun, J. C., Helton, A. M., Briggs, M. A., & Kurylyk, B. L. (2021). An ecohydrological typology for thermal refuges in streams and rivers. *Ecohydrology*, *14*, e2295. https://doi.org/10.1002/eco.2295

Sytsma, A., Bell, C., Eisenstein, W., Hogue, T., & Kondolf, G. M. (2020). A geospatial approach for estimating hydrological connectivity of impervious surfaces. *Journal of Hydrology*, *591*, 125545. https://doi.org/10.1016/j.jhydrol.2020.125545

Tesoriero, A. J., Duff, J. H., Saad, D. A., Spahr, N. E., & Wolock, D. M. (2013). Vulnerability of streams to legacy nitrate sources. *Environmental Science & Technology*, *47*, 3623–3629. https://doi.org/10.1021/es305026x

Torgersen, C. E., Faux, R. N., McIntosh, B. A., Poage, N. J., & Norton, D. J. (2001). Airborne thermal remote sensing for water temperature assessment in rivers and streams. *Remote Sensing of Environment*, *76*, 386–398. https://doi.org/10.1016/S0034-4257(01)00186-9

U.S. Geological Survey. (2016). Water data for the Nation: U.S. Geological Survey National Water Information System database. Accessed December 13, 2023 https://doi.org/10.5066/F7P55KJN

U.S. Geological Survey. (2019a). The StreamStats program. online at https://streamstats.usgs.gov/ss/, Accessed on March, 23 2022

U.S. Geological Survey. (2019b). National Hydrography Dataset (ver. USGS National Hydrography Dataset Best Resolution (NHD) for Hydrologic Unit (HU) 8-2001. (published 20191002)), accessed March, 23 2022 at https://www.usgs.gov/national-hydrography/access-national-hydrography-products

van Balen, R. T., Kasse, C., & De Moor, J. (2008). Impact of groundwater flow on meandering; example from the Geul River, The Netherlands. *Earth Surface Processes and Landforms*, *33*, 2010–2028. https://doi.org/10.1002/esp.1651

Walsh, C. J., Roy, A. H., Feminella, J. W., Cottingham, P. D., Groffman, P. M., & Morgan, R. P. (2005). The Urban Stream Syndrome: Current Knowledge and the Search for a Cure. https://doi.org/10.1899/04-028.1

Wawrzyniak, V., Piégay, H., Allemand, P., Vaudor, L., Goma, R., & Grandjean, P. (2016). Effects of geomorphology and groundwater level on the spatio-temporal variability of riverine cold water patches assessed using thermal infrared (TIR) remote sensing. *Remote Sensing of Environment*, *175*, 337–348. https://doi.org/10.1016/j.rse.2015.12.050

Winter, T. C., Harvey, J. W., Franke, O. L., & Alley, W. M. (1998). Ground water and surface water: A single resource (USGS numbered series No. 1139), ground water and surface water: A single resource, circular. U.S. Geological Survey. https://doi.org/10.3133/cir1139

Yearsley, J. R., Sun, N., Baptiste, M., & Nijssen, B. (2019). Assessing the impacts of hydrologic and land use alterations on water temperature in the Farmington River basin in Connecticut. *Hydrology and Earth Systems Sciences*, *HESS*, *23*, 4491–4508. https://doi.org/10.5194/hess-23-4491-2019

SUPPORTING INFORMATION

Additional supporting information can be found online in the Supporting Information section at the end of this article.

How to cite this article: Jackson, K. E., Moore, E. M., Helton, A. M., Haynes, A. B., Barclay, J. R., & Briggs, M. A. (2024). Exploring landscape and geologic controls on spatial patterning of streambank groundwater discharge in a mixed land use watershed. *Hydrological Processes*, *38*(3), e15112. https://doi.org/10.1002/hyp.15112

10991085, 2024, 3, Downloaded from https://onlinelibrary.wiley.com/doi/10.1002/hyp.15112, Wiley Online Library on [26/11/2025]. See the Terms and Conditions (https://onlinelibrary.wiley.com/terms-and-conditions) on Wiley Online Library for rules of use; OA articles are governed by the applicable Creative Commons License